IEEE Access
Multidisciplinary | Rapid Review | Open Access Journal

Received 12 March 2024, accepted 30 March 2024, date of publication 11 April 2024, date of current version 29 April 2024.

Digital Object Identifier 10.1109/ACCESS.2024.3387533

RESEARCH ARTICLE

Pipelined Structure in the Classification of Skin Lesions Based on Alexnet CNN and SVM Model With Bi-Sectional Texture Features

V. S. S. BALA TRIPURA SATHVIKA[1], NAGILLA ANMISHA[1], VADA THANMAYI[1], M. SUCHETHA[2], (Senior Member, IEEE), D. EDWIN DHAS[1], S. SEHASTRAJIT[2], AND SATHYANARAYANAN N. AAKUR[3], (Member, IEEE)

[1]Vellore Institute of Technology, Chennai 600127, India
[2]Centre for Healthcare Advancement, Innovation and Research, Vellore Institute of Technology, Chennai 600127, India
[3]Department of Computer Science and Software Engineering, Auburn University, Auburn, AL 36849, USA

Corresponding author: M. Suchetha (suchetha.m@vit.ac.in)

ABSTRACT The classification of skin lesions is crucial because it increases the likelihood that malignant skin lesions will be discovered early on, allowing for more effective treatment. Due to the abundance of lesion images and the possibility of human error, early detection can be difficult for dermatologists. This work aims to classify skin lesions using two pipelines that were designed using support vector machine (SVM) and AlexNet convolutional neural network (CNN) models. Pipeline-1 uses the AlexNet CNN, while pipeline-2 proposes a bisectional feature extraction approach with an SVM model. The skin lesion images are initially preprocessed and the lesion regions are segmented. The lesion regions are further subdivided into four regions based on the intensity mapping function. The bisectional features are then extracted from the subdivided regions and the extracted features are trained with the SVM model. The dataset used in the experiment is the HAM-10000 dataset and the PAD-UFES-20 dataset, which consists of dermatoscopic skin lesions images. Based on the models' accuracy, sensitivity, DCI, specificity, and F1-score, the experiment's findings will be assessed for five different skin lesion conditions. By accurately and effectively classifying skin lesions, the study's findings will help in the diagnosis and treatment of skin disorders. The SVM pipeline performs better than the AlexNet CNN pipeline where the SVM pipeline and AlexNet CNN pipeline result in an accuracy of 98.66% and 97.68% respectively for the HAM-10000 dataset. The AlexNet CNN and SVM pipeline structure results in an accuracy of 96.87% and 98.10% respectively for the PAD-UFES-20 dataset.

INDEX TERMS Skin lesions, support vector machine, deep learning, AlexNet, CNN.

I. INTRODUCTION

Skin lesions are abnormal growths or changes to the skin that can be brought on by a number of things, such as illnesses, traumas, allergies, and infections. They can take on a variety of shapes and sizes, from little bumps, blisters, and moles to bigger regions of discoloration and growths with irregular shapes. Depending on the type and severity of the skin lesions which can be benign or malignant it may be necessary to seek medical assistance [1]. In order to diagnose and treat skin problems as well as to avoid consequences like infections and skin cancer, it is essential to understand the features of skin lesions. In reality, according to various studies, skin diseases are among the most prevalent human illnesses, affecting people of all ages, genders, and cultures. The economic and health implications of skin cancer are significant. For recognizing early skin disorders, it is advised to be aware of new or altering skin growths. The possibility of early-stage skin cancer detection and doing it through automatic skin lesion classification systems having performance at least or greater than traditional detection methods is a rather promising challenge. Because the most fatal type of skin lesion, Melanoma, can have a 5-year survival rate of up to 99% with early identification. One of

The associate editor coordinating the review of this manuscript and approving it for publication was Sotirios Goudos.

© 2024 The Authors. This work is licensed under a Creative Commons Attribution-NonCommercial-NoDerivatives 4.0 License.
For more information, see https://creativecommons.org/licenses/by-nc-nd/4.0/

the most widely used approaches for analyzing skin lesions is the ABCD analysis [2].

Traditional methodologies such as eye inspection and dermoscopy, as well as more contemporary techniques incorporating machine learning algorithms, were used to classify skin lesions. The ability of these algorithms to effectively categorize skin lesions as benign or malignant has shown considerable potential. This will help doctors to identify Melanoma in its early stages and potentially save lives. Convolutional neural networks (CNNs) and Support vector machines (SVMs), two of the most frequently used methods, have been applied to numerous datasets with promising results. To detect psoriasis with the help of traits such as skin tone and texture, many used [3] feed-forward neural networks. For a more accurate and reliable result, the paper relied on both skin color and texture data. The input images were classified as psoriasis or non-psoriasis and implemented using feed-forward neural networks. The system performed admirably during the generalization and training phases of the neural network. They used psoriasis disease as an example in this work to assess how well the suggested skin texture recognition algorithm can distinguish between healthy and sick skin. The difficulty of precisely and automatically categorizing skin lesions was addressed by the authors Khan et al. [4]. This is a significant concern in the timely detection and avoidance of malignancies of the skin. They contend that because of the great diversity and intricate nature of skin diseases, conventional methods for machine learning face shortcomings in this domain. They took advantage of teledermatology, which ranks among the most eminent telemedicine and digital health applications. Telecommunication methods are used in this industry to transmit clinical data to other professionals. Limiting unnecessary medical references and prioritizing dermatology problems are additional benefits. A number of authors also spoke regarding the prospective advantages of automated diagnosis solutions leveraging deep learning (DL) based techniques [5] like CNNs and EfficientNet architecture, including increased certainty of diagnosis, decreased physician effort, and happier patients [6]. Their work outlines potential paths for subsequent studies, including the creation of sizable and varied datasets, the analysis of multimodal strategies, and the examination of explainable AI methods for categorization.

The contribution of the work is briefly summarized below. In order to create a sophisticated system for classifying skin lesions, this work will focus on deploying deep learning along with a few image processing approaches to images extracted from the dataset. Images are processed using two different pipelines after employing some pre-processing approaches to refine contrast and remove hairs. The first one employs the AlexNet convolutional neural network (CNN) for image classification, while the second employs the support vector machine classifier that is trained using features derived from the lesion regions. In particular, the second pipeline uses a segmentation technique to divide the image into regions of interest (ROI) using the k-means clustering algorithm, then establishes the ROI that best represents the lesion among all of the ROIs, and subsequently performs feature extraction based on ABCDT analysis to utilize the extracted features for the training of the SVM machine learning model. Since the pipelines offer distinct approaches to categorizing dermatoscopic images, it is a key objective of this work to assess and compare the outcomes and performance of both approaches in order to thoroughly compare shallow and deep learning approaches.

The sections in the work are as follows. Section II discusses a few of the related works in the classification of skin lesions. Section III elaborates on the working of the two pipeline structures in the classification of skin lesions, Section IV analyzes the results obtained in the classification of the skin lesions and finally, the conclusion of the proposed skin lesion classification is provided in Section V.

II. RELATED WORKS

Artificial intelligence plays an ultimate role in the automatic classification of medical images of different modalities [7], [8]. The scheme [9] first divided the image through distinct component analysis into pigment and blood elements before segmenting the vascular architecture of the lesion. By doing this, the influence of melanin on vessel permeability is eliminated. The blood's hemoglobin portion is subsequently aggregated into regular, pigmented, and erythema zones. The erythema cluster is then subjected to several levels of shape filters. Consequently, the segmentation's specificity and sensitivity were outstanding. The author Arifin et al. [10] proposed k-means clustering and color gradient technique for employing color skin scans to diagnose dermatological conditions. The approach has two interdependent steps the first identifies diseases, while the second identifies the skin anomalies. The approach depends on visual input, such as patient medical history and high-resolution color photographs. To identify the sick skin through machine intervention, the approach employs color image processing methods namely color gradient and k-means clustering. The technique uses feed-forward back-propagation artificial neural networks to categorize diseases. When tested on a total of 2055 diseased spots in 704 skin lesion images for 6 illnesses, the approach showed a diseased skin detection accuracy and disease identification accuracy of 95.99% and 94.016% respectively.

HAM10000 dataset is used to test the above-mentioned approach for multi-class skin disease classification using transfer learning and data augmentation techniques which address the dataset's significant class imbalances [11]. This study suggests a transfer learning-based model that makes use of an Xception model that has already been trained. The addition of layers, including a pooling layer, two thick layers, and one dropout layer, modifies the Xception model. For seven groups of skin diseases, a new fully connected (FC) layer has been added in place of the original FC layer. According to the latest data, the scheme can accurately classify skin conditions 96.40% of the time. With

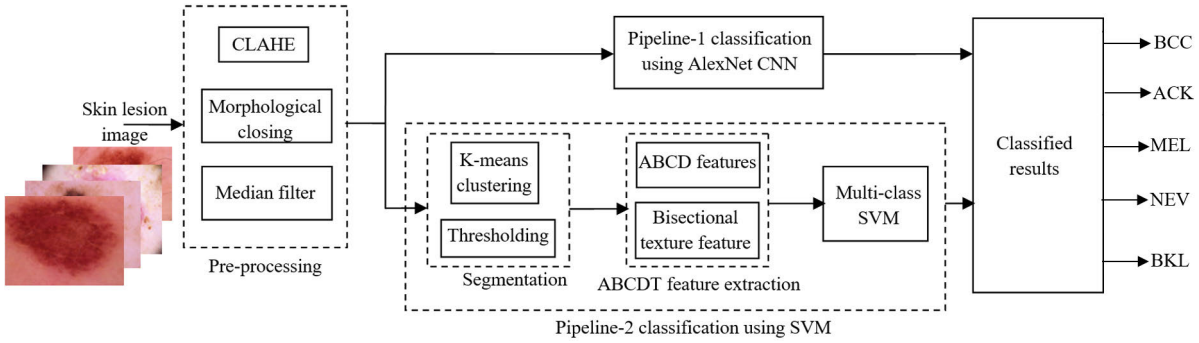

FIGURE 1. Proposed framework of skin lesion classification.

F1-score, sensitivity, and precision values of 98%, 97%, and 99%, respectively, the model performs best on benign keratosis. Few proposed a skin disease identification method using machine learning for dataset training and SVM for classification [12]. They used publicly available databases such as DermWeb and Dermnet to collect images. The scheme is based on vectors and pixel classification of the images and it classifies the images into five categories of diseases: Psoriasis, Melanoma, Rosacea, Vitiligo, and Xanthelasma. The author Allugunti introduced a CNN model for skin disease classification [13] with the dataset taken from the website dermnetnz.org. This CNN method is a two-stage learning platform that provides an overall accuracy of 88.83% beats the other classification algorithms random forest (RF) and decision tree (DT) which have an accuracy in the 65%-75% range. It also significantly reduces the computational effort required. Its drawback is that it is tested only on a single dataset. For the classification of Nevus and Melanoma from skin images the approach [14] implemented an improved K-mean clustering approach after applying a Gaussian filter to eliminate noise from images of skin lesions. Textural and color features that were collected from the lesion are combined to generate a hybrid feature vector, and an SVM is then utilized to categorize the skin cancer as Nevus or Melanoma. The DERMIS dataset is used to test the suggested methodology, which yielded a 96% accuracy rate. The purpose of the scheme is to evaluate the segmentation method, extract pertinent characteristics, and evaluate the classification outcomes.

CNNs have shown tremendous promise in assisting the detection and treatment of skin illnesses, according to recent research [15]. These customized deep-learning algorithms can correctly categorize skin lesions into various groups, enabling quicker and more precise diagnoses. Another study [16] created a novel framework based on CNNs for identifying various skin conditions in a clinical setting. This method demonstrated a high accuracy rate of 90.5% in detecting skin conditions, such as basal cell Carcinoma and Melanoma. In order to increase the precision and efficiency of diagnosis, automated image-based methods that leverage machine learning categorization, such as CNNs, have also been suggested [17]. The image classification performance of AlexNet CNN is renowned for being exceptional [18]. Rectified linear units (ReLU), which train more quickly than the common *tanh* function used in other CNNs [19], are one of the benefits AlexNet has over other CNNs. Additionally, AlexNet makes use of overlapping pooling, which can lower errors by roughly 0.5% [19]. To lessen overfitting, AlexNet also employs data augmentation and dropout techniques [19]. Due to these characteristics, AlexNet is a powerful model for object recognition, including the classification of skin lesions.

Support Vector Machines (SVMs) have demonstrated significant promise in the classification of skin lesions and the treatment of skin illnesses [20]. Machine learning algorithms called SVMs can be applied to categorization jobs. SVMs operate by locating the ideal hyperplane that divides various data classes. When dealing with high-dimensional data, such as medical imaging, they are especially useful. SVMs have been used to categorize skin lesions as either benign or Melanoma lesions in conjunction with deep learning-based automatic skin lesion segmentation [20]. In another study, three different types of skin lesions were classified with a higher accuracy rate using SVM and GLCM [21]. In a computerized procedure for detecting skin diseases using long short-term memory (LSTM) and MobileNet V2 based on deep learning, SVM has also been utilized as a classifier [22]. SVMs have demonstrated considerable promise for assisting in the diagnosis and treatment of skin ailments.

The work proposes two pipeline structures for the classification of the skin lesion. Pipeline-1 uses an AlexNet CNN where the skin lesion features are extracted by the model itself. Pipeline 2 uses the ABCDT features to classify the skin lesion categories. More specifically the pipeline-2 structure proposes a Bisectional texture feature that highly differentiates the skin lesion image categories.

III. PROPOSED METHOD

The diagrammatic representation of the proposed skin lesion classification that uses the two pipeline structures is illustrated in Fig. 1. The proposed approach can classify the skin lesion images into five classes namely

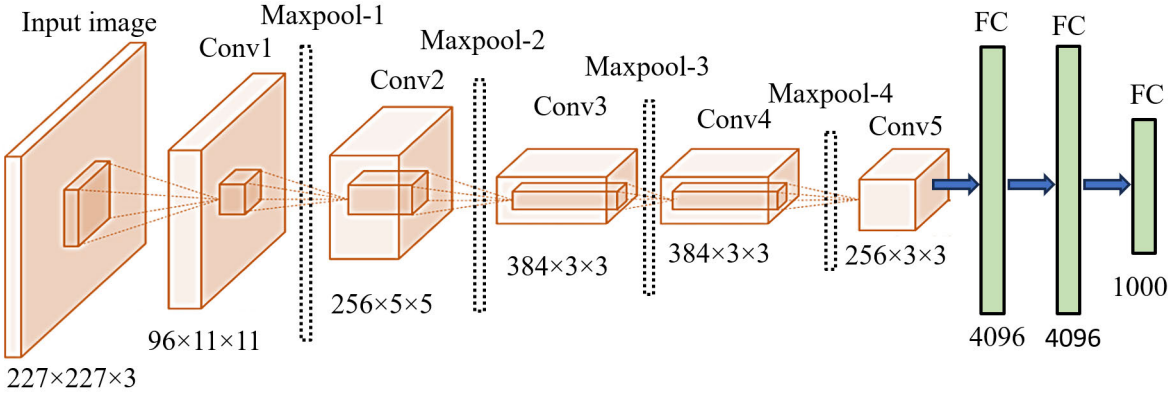

FIGURE 2. Architecture of AlexNet CNN for skin lesion classification.

basal cell carcinoma (BCC), Actinic Keratoses (ACK), Melanoma (MEL), Melanocytic nevi (NEV), and Benign Keratosis (BKL). The different stages included in the proposed skin lesion classification include (a) Pre-processing (b) Pipeline-1: Classification using AlexNet convolutional neural network, and (c) Pipeline-2: Classification of features using support vector machine.

A. PREPROCESSING

Preprocessing the dataset entails scaling and normalizing the lesion images as the first step. Preprocessing comprises three different steps such as contrast-limited adaptive histogram equalization (CLAHE), morphological closing, and median filtering. An image processing method that improves contrast is called CLAHE. To enhance the visual quality of images, it is a modified version of the conventional histogram equalization technique that is widely utilized in medical imaging, remote sensing, and computer vision applications [23]. Morphological closing is a common image-processing technique that has also been used to classify skin lesions. Several approaches for classifying skin lesions were examined and discovered that morphological closing is useful for enhancing classification model accuracy [24]. In applications involving medical imaging, the method has also been used with CLAHE [25]. A structuring element is used in morphological closing, which can be used to fill in gaps and remove small items from an image by first applying a dilation operation to it. Better feature extraction as a result can raise the precision of classification models. The median filter is a commonly used technique in image processing, including skin lesion classification. It works by replacing each pixel's value with the median of its neighboring pixels, effectively removing noise and smoothing the image. This technique has been found to improve classification accuracy, making it an essential tool in the medical imaging field. In this work, we use CLAHE to improve the contrast and brightness of the images, and we use morphological closure to clean up stains and hairs from equalized images using a disk of radius 7. The median filter is used to filter the image after morphological closing to quickly and accurately perform linear interpolation.

B. PIPELINE 1: CLASSIFICATION USING ALEXNET CNN

There are various phases involved in classifying skin lesions using the AlexNet convolutional neural network. AlexNet is a Convolutional neural network (CNN) architecture that has 5 convolutional layers and 3 FC layers [26]. Local response normalization, dropout regularization, and ReLU activation functions are all included in the architecture of AlexNet. While the fully connected layers of AlexNet learn high-level features like object recognition, the convolutional layers of the network learn to detect low-level features like edges and corners. With approximately 60 million parameters, AlexNet has a much bigger number of parameters than earlier models [26]. The AlexNet CNN, which has been demonstrated to perform better in the categorization of skin lesions, is used in the second stage to develop the model architecture. The model is trained and validated with the use of preprocessed images in the third stage. The model's accuracy is tested using a different test dataset in the fourth stage. The model will then be used in a clinical setting to diagnose and treat skin conditions. Fig. 2 illustrates the architecture of AlexNet CNN used in the proposed work for skin lesion classification.

C. PIPELINE 2: CLASSIFICATION USING THE SVM MODEL BASED ON ABCDT FEATURES

The pipeline-2 includes three stages for classifying the skin lesions which include stages such as segmentation and extraction of ABCDT features followed by a multi-class SVM classifier.

1) SEGMENTATION

The segmentation aims to segment the lesion region of interest (RoI) by eliminating other skin regions. The work uses the segmentation presented in the scheme [27]. The proposed approach uses the k-means clustering approach followed by the thresholding [27] to segment the lesion

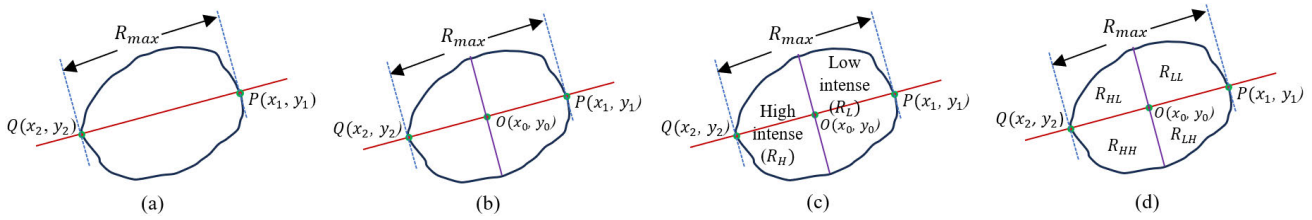

FIGURE 3. Estimation of the region in extracting the bisectional texture features.

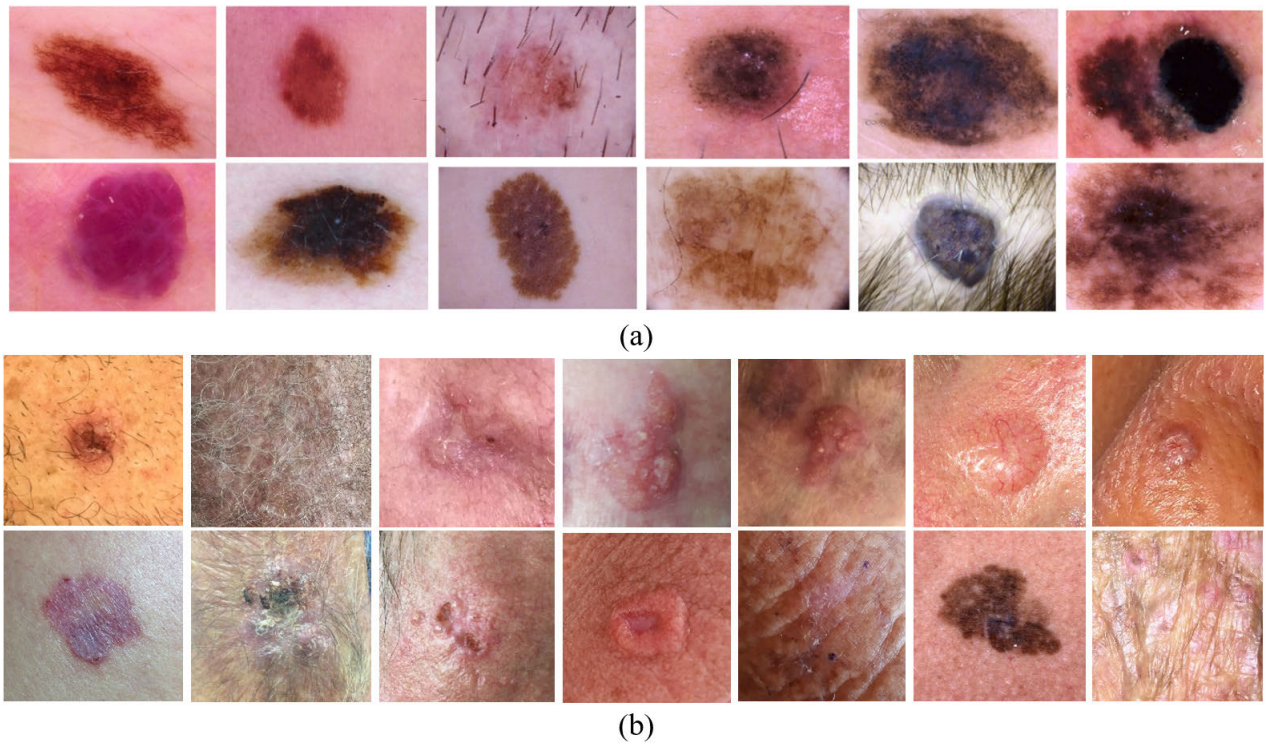

FIGURE 4. Sample skin lesion images used for analysis (a) HAM10000 dataset (b) PAD-UFES-20 dataset.

region. The k-means clustering algorithm is applied after converting the Pre-processed RGB skin lesion image to grayscale. The proposed scheme uses the number of clusters as 2 to segment the lesion region into foreground and background. The foreground region is then thresholded and dilated by morphological processing to obtain the segmented lesion region.

2) ABCDT FEATURE EXTRACTION

The proposed work uses the ABCDT features relating to asymmetry (A), border irregularity (B), color variation (C), the diameter of the lesion (D) [2], and texture (T) will be extracted using the ABCDT approach, which is based on the ABCD analysis. The features such as asymmetry, border irregularity, color variation, and diameter are estimated for the single lesion region. Two features are extracted to obtain the asymmetry of the lesion region which includes the lengthening and asymmetry index. The border irregularity feature is estimated using the features namely density index, pigmentation transition, edge abruptness, fractal dimension, and compactness index. The color variation feature is estimated using the correlation between photometry and geometry. The color homogeneity feature also plays an important role in estimating the color variation. The average diameter is estimated after calculating different chord that passes through the midpoint of the lesion region. Let F_A, F_B, F_C, and F_D represent the ABCD features that are estimated. However, the texture feature is estimated as provided in the following section.

3) BI-SECTIONAL TEXTURE FEATURES

For estimating the bi-sectional texture features, the maximum diameter is initially estimated on the lesion region $R(x, y)$. Let the two boundary points that correspond to the maximum diameter be represented as $P(x_1, y_1)$ and $Q(x_2, y_2)$ as illustrated in Fig. 3(a). Let the maximum diameter be represented

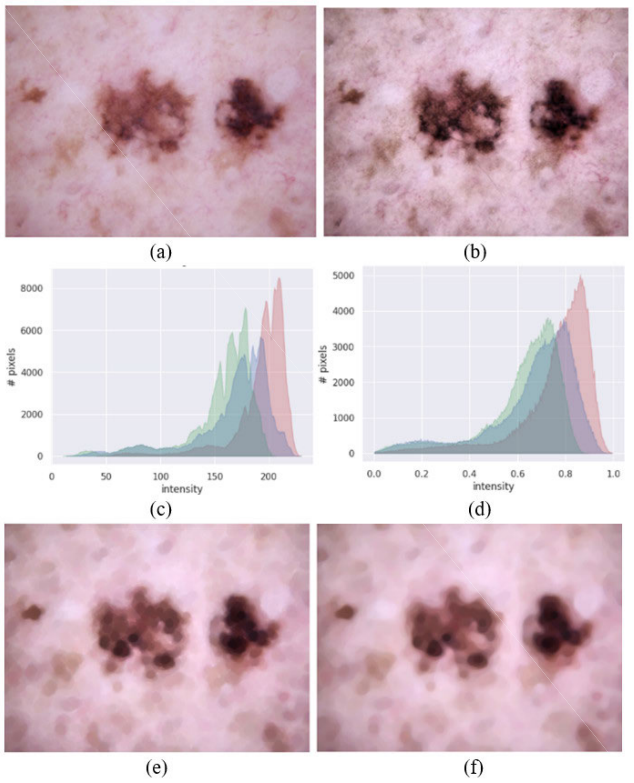

FIGURE 5. Experimental results obtained for the lesion image record ISIC0030501 (a) Original image (b) Histogram equalized output with CLAHE (c) Histogram of the original image (d) Histogram of Histogram equalized image (e) Result obtained after morphological closing (f) Result obtained after median filtering.

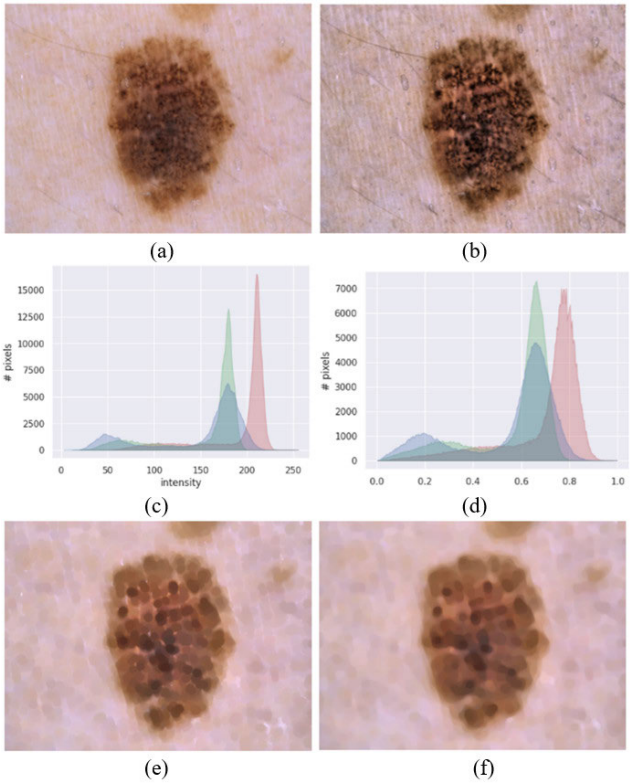

FIGURE 6. Experimental results obtained for the lesion image record ISIC0024870 (a) Original image (b) Histogram equalized output with CLAHE (c) Histogram of the original image (d) Histogram of histogram equalized image (e) Result obtained after morphological closing (f) Result obtained after median filtering.

as R_{max}. The midpoint $O(x_0, y_0)$ is then estimated from the extreme points $P(x_1, y_1)$ and $Q(x_2, y_2)$ using the relation

$$(x_0, y_0) = \left(\frac{x_1 + x_2}{2}, \frac{y_1 + y_2}{2}\right) \tag{1}$$

An perpendicular line is constructed with respect to $P(x_1, y_1)$ and $Q(x_2, y_2)$ on the centre point $O(x_0, y_0)$ as illustrated in Fig. 3(b). The newly formed perpendicular line constructs two regions $R_1(x, y)$ and $R_2(x, y)$. From the $R_1(x, y)$ and $R_2(x, y)$ a high-intense and low-intense region were detected. Let the mean threshold intensity of the two regions $R_1(x, y)$ and $R_2(x, y)$ be T_{R_1} and T_{R_2} respectively which can be estimated using the relations,

$$T_{R_1} = \frac{1}{N_{R_1}} \sum_{x=i_1, y=j_1} R_1(x, y) \tag{2}$$

$$T_{R_2} = \frac{1}{N_{R_2}} \sum_{x=i_2, y=j_2} R_2(x, y) \tag{3}$$

where (i_1, j_1) represents the index of the pixels in the region $R_1(x, y)$ and (i_2, j_2) represents the index of the pixels in the region $R_2(x, y)$. N_{R_1} and N_{R_2} represents the number of pixels in the region $R_1(x, y)$ and $R_2(x, y)$ respectively as illustrated in Fig. 3(c). A region $R_1(x, y)$ is considered a highly intense region, and $R_2(x, y)$ is considered as a low intense region if the region satisfies the condition $T_{R_1} \geq T_{R_2}$. Similarly, the region $R_1(x, y)$ is considered as a low intense region, and $R_2(x, y)$ is considered as a high intense region if the region satisfies the condition $T_{R_1} < T_{R_2}$. Let the high intense region be represented as R_H, while the low intense region be represented as R_L. The high intense region R_H is again partitioned in to two region namely R_{H1} and R_{H2} using the mean intensity values $T_{R_{H1}}$ and $T_{R_{H2}}$ respectively estimated as,

$$T_{R_{H1}} = \frac{1}{N_{H1}} \sum_{x=i_3, y=j_3} R_{H1}(x, y) \tag{4}$$

$$T_{R_{H2}} = \frac{1}{N_{H2}} \sum_{x=i_4, y=j_4} R_{H2}(x, y) \tag{5}$$

where (i_3, j_3) represents the index of the pixels in the region $R_{H1}(x, y)$ and (i_4, j_4) represents the index of the pixels in the region $R_{H2}(x, y)$. N_{H1} and N_{H2} represents the number of pixels in the region $R_{H1}(x, y)$ and $R_{H2}(x, y)$ respectively. A region in R_{H1} is said to be a high intense region of R_H, if $T_{R_{H1}} \geq T_{R_{H2}}$, else the region is considered as low intense region of R_H. Let the high and low intense regions of R_H be represented as R_{HH} and R_{HL} respectively.

Similarly, the low intense region R_L is again partitioned in to region namely R_{L1} and R_{L2} using the mean intensity values

$$T_{R_{L1}} = \frac{1}{N_{L1}} \sum_{x=i_5, y=j_5} R_{L1}(x, y) \tag{6}$$

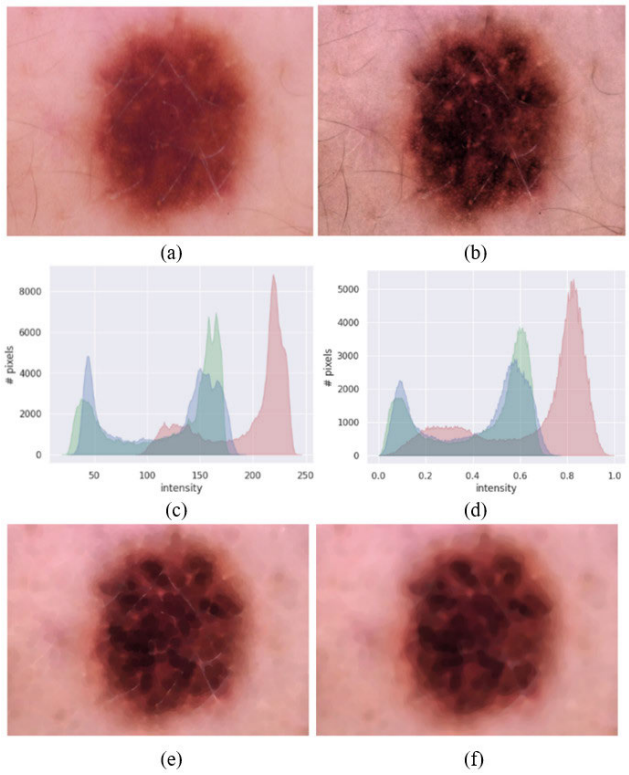

FIGURE 7. Experimental results obtained for the lesion image record ISIC0024894 (a) Original image (b) Histogram equalized output with CLAHE (c) Histogram of the original image (d) Histogram of histogram equalized image (e) Result obtained after morphological closing (f) Result obtained after median filtering.

$$T_{R_{L2}} = \frac{1}{N_{L2}} \sum_{x=i_6, y=j_6} R_{L2}(x, y) \tag{7}$$

where (i_5, j_5) represents the index of the pixels in the region $R_{L1}(x, y)$ and (i_6, j_6) represents the index of the pixels in the region $R_{L2}(x, y)$. N_{L1} and N_{L2} represents the number of pixels in the region $R_{L1}(x, y)$ and $R_{L2}(x, y)$ respectively. A region in R_{L1} is said to be a highly intense region of R_L if $T_{R_{L1}} \geq T_{R_{L2}}$, else the region is considered an as low intense region of R_L. Let the high and low intense regions of R_H be represented as R_{LH} and R_{LL} respectively.

The texture feature [28] is estimated from the four regions R_{HH}, R_{HL}, R_{LH} and R_{LL} as illustrated in Fig. 3(d). Let the number of features obtained from the highly intense region R_H be N_s. The proposed approach extracts a greater number of features from the high-intense region R_H, while it extracts a lesser number of features from the lower intense R_L region. Let N_s and N_g represent the number of texture features extracted from the high-intense and low-intense regions respectively. The number of features N_s and N_g are related using the feature strength index β as

$$N_g = \beta N_s \tag{8}$$

where $0 < \beta \leq 1$. Let the texture features extracted from the region R_{HH} and R_{HL} be represented as $f_{HH,k}$ and $f_{HL,k}$ respectively, where $k = 1, 2 \ldots . N_s$. Similary the texture features extracted from the region R_{LH} and R_{LL} be represented as $f_{LH,l}$ and $f_{LL,l}$ respectively, where $l = 1, 2 \ldots . N_g$. The feature that represent the texture variation between $f_{HH,k}$ and $f_{HL,k}$ is represented as

$$F_H = \hat{f}_{H,k} = f_{HH,k} - f_{HL,k} \tag{9}$$

Similarly, the feature that represent the texture variation between $f_{LH,k}$ and $f_{LL,k}$ is represented as

$$F_L = \hat{f}_{L,k} = f_{LH,l} - f_{LL,l} \tag{10}$$

The features F_H and F_L represent the bisectional texture features. Thus the features extracted from a single lesion image are represented as

$$F = [F_A, F_B, F_C, F_D, F_T] = [F_A, F_B, F_C, F_D, F_H, F_L] \tag{11}$$

4) MULTI-CLASS SVM CLASSIFIER

SVM is a well-liked machine learning scheme used for regression analysis and classification purposes. The concept of supervised learning can be applied to categorizing both linear and non-linear data. Finding the hyperplane that best categorizes the data into distinct classes is how SVM operates [20]. To reduce its sensitivity to noisy data, the hyperplane is chosen to maximize the margin between the two classes. SVMs are frequently employed across a broad spectrum of applications, including bio-informatics, text classification, and picture classification. The SVM models are renowned for their great accuracy and ability to handle huge datasets with ease. The lesion identification technique is then used to identify the area where the lesion is located. The SVM classifier is then employed and the ideal setting for each of its hyperparameters is discovered. For the selection of N_s number of A, B, C, D, and T features, the covariance between the extracted features is initially estimated. The features that have the top N_s number of covariance values are used for training or classifying the SVM model. The features obtained from the skin lesion images are trained using the multi-class SVM classifier with 5 classes. In the testing phase, the test image undergoes all processes involved in the training phase to obtain the features. The feature obtained from the test image is fed to the trained SVM model to obtain the classified lesion category. Performance evaluation over the test set would be the last step in this pipeline. Metrics obtained from both pipelines are compared and evaluated.

IV. EXPERIMENTAL RESULTS

The evaluation of proposed skin lesion classification algorithm was evaluated using the HAM 10000 dataset [29] and the PAD-UFES-20 dataset [30]. The HAM10000 dataset is composed of 11,527 dermatoscopic images of skin lesions exhibiting pigment, including benign and malignant lesions. The International Skin Imaging Collaboration (ISIC) generated the collection, which features images of common skin lesions. The images were collected from different

TABLE 1. Number of images used for analysis in each class before and after augmentation.

Augmentation	Dataset	BCC	ACK	MEL	NEV	BKL
Before	HAM 10000	514	327	1113	6705	1099
	PAD-UFES-20	845	730	52	244	235
After	HAM 10000	2570	1635	5565	6705	5495
	PAD-UFES-20	4225	3650	260	1220	1175

TABLE 2. Number of images used in the training and testing phases.

Phase	Dataset	BCC	ACK	MEL	NEV	BKL
Training	HAM 10000	1799	1145	3896	4694	3847
	PAD-UFES-20	2958	2555	182	854	823
Testing	HAM 10000	771	490	1669	2011	1648
	PAD-UFES-20	1267	1095	78	366	352

sources and were labeled by experts in dermatology. The HAM10000 dataset is widely used in research to develop and evaluate algorithms for automated skin lesion classification. The PAD-UFES-20 dataset contains 2298 skin lesion images collected from 1,373 patients. A few of the sample images obtained from the HAM10000 dataset and PAD-UFES-20 are presented in Fig. 4.

We have used the skin lesion classes namely basal cell carcinoma (BCC), Actinic Keratoses (ACK), Melanoma (MEL), Melanocytic nevi (NEV), and Benign Keratosis (BKL). To fit the model, image augmentation such as Image rotation by 90°, Image rotation by 270°, vertical flipping, and horizontal flipping. The number of images used in each class from the two datasets before and after image augmentation is depicted in Table 1.

Let the true negatives, true positives, false negatives and false positives obtained in the lesion classification be C_{TN}, C_{TP}, C_{FN} and C_{FP} respectively. The classification performance of the proposed skin lesion classification was evaluated with the performance measures namely F1-score, sensitivity (Sen), specificity (Spe), accuracy (Acc), and dice coefficient index (DCI) with the relations

$$F1 - score = \frac{C_{TP}}{C_{TP} + 0.5 \times (C_{FN} + C_{FP})} \tag{12}$$

$$Sensitivity = \frac{C_{TP}}{C_{TP} + C_{FN}} \tag{13}$$

$$Specificity = \frac{C_{TN}}{C_{TN} + C_{FP}} \tag{14}$$

$$Accuracy = \frac{C_{TN} + C_{TP}}{C_{TN} + C_{FP} + C_{FN} + C_{FP}} \tag{15}$$

$$DCI = \frac{2 \times C_{TP}}{2 \times C_{TP} + C_{FP} + C_{FN}} \tag{16}$$

Table 2 depicts the number of skin lesion images used in the training and testing of the proposed skin lesion algorithm. From the augmented images 70% of the images are used for training, and the rest 30% of lesion images are used for testing the proposed model.

Fig. 5 illustrates the experimental result obtained for the lesion record ISIC0030501. This includes the result after the contrast enhancement, followed by morphological operation, and median filtering. The histogram of the original image gets broadened as a result of histogram equalization. The result of morphological operation followed by median filtering eliminates the artifacts caused due to the presence of hair. Fig. 6, and Fig. 7 illustrate the experimental result obtained for the lesion image record ISIC0024870 and ISIC0024894 respectively. Fig. 7 (f) shows the absence of hair artifacts present in the lesion image shown in Fig. 7 (a). Fig. 8 shows the experimental results obtained in the segmentation of skin lesions by the pipeline-2 section. This shows the k-means clustering results followed by the morphological and thresholding operations. The proposed segmentation can segment the weak boundaries of the lesion region. The extraction of features on the complete lesion region improves the performance in lesion classification. The procedures to improve segmentation include filling in small holes, deleting small objects with an area smaller than 80 pixels, and, if applicable, removing regions connected to the picture contours. The lesion identification method completes the segmentation process by identifying the region that represents the lesion. The findings show that the segmentation technique adopted in this work was effective at locating the regions of interest and determining which one corresponds to the lesion. The outcomes show that the segmentation technique utilized in this study was reliable at locating the regions of interest and determining which one corresponds to the lesion.

The performance of the proposed skin lesion classification algorithm was compared with the recent skin lesion classification schemes namely multi-features [31], multi-scale attention [32], feature fusion [33], soft attention [34], fusionM4Net [35], and contractive learning [36].

For the HAM-10000 dataset, the proposed pipeline-1 results in an F1-score, specificity, sensitivity, accuracy, and DCI of 94.38%, 93.21%, 94.63%, 97.21%, and 95.82% respectively. The performance of the proposed pipeline-2 which uses the bi-sectional features with the SVM classifier has a higher performance than the pipeline-1 approach in the case of the HAM-10000 dataset. The pipeline-2 approach results in an F1-score, specificity, sensitivity, accuracy, and DCI of 95.96%, 96.58%, 95.82%, 98.66%, and 95.12% respectively.

In the case of the HAM-10000 dataset, the accuracy of the pipeline-2 approach is 0.98% higher than the pipeline-1 approach. With the recent lesion classification schemes, the pipeline-1 approach provides higher accuracy than all the schemes other than the feature fusion approach. However, the pipeline-2 approach has higher accuracy than the recent

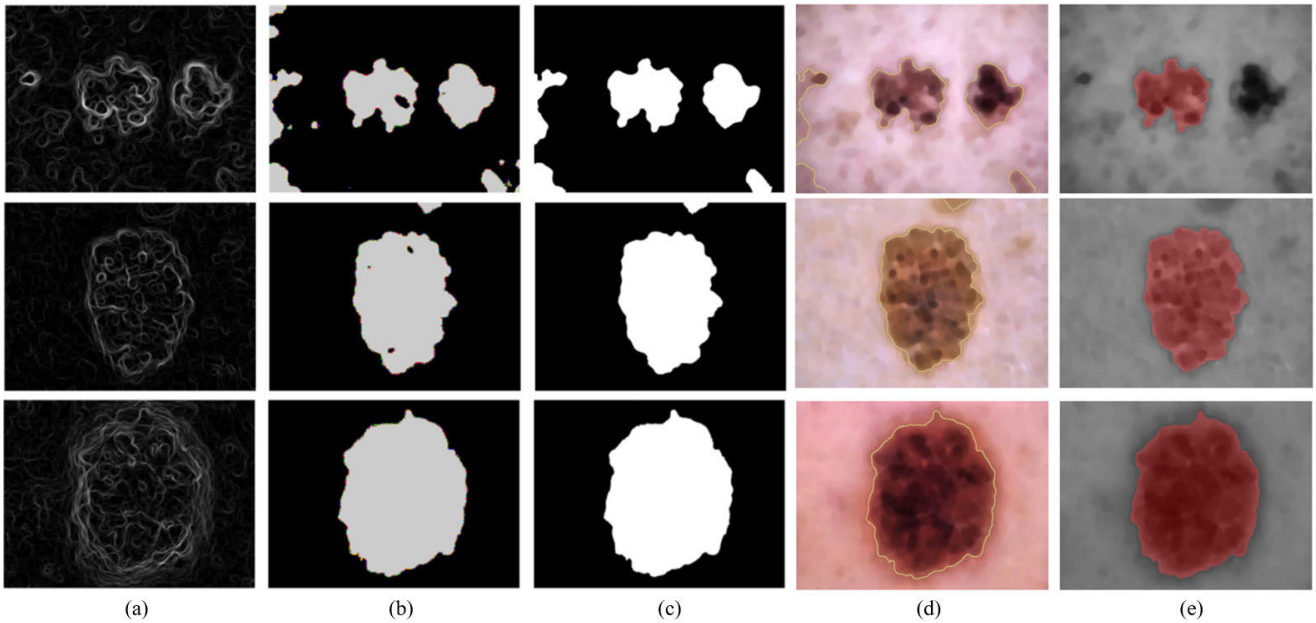

FIGURE 8. Experimental results obtained in the segmentation of skin lesion (a) Results obtained by k-means clustering (b) Thresholding of k-means output (c) Result of morphological operation (d)-(e) Isolation of lesion region (row1) Record-ISIC0030501 (row2) Record-ISIC24870 (row3) Record-ISIC0024894.

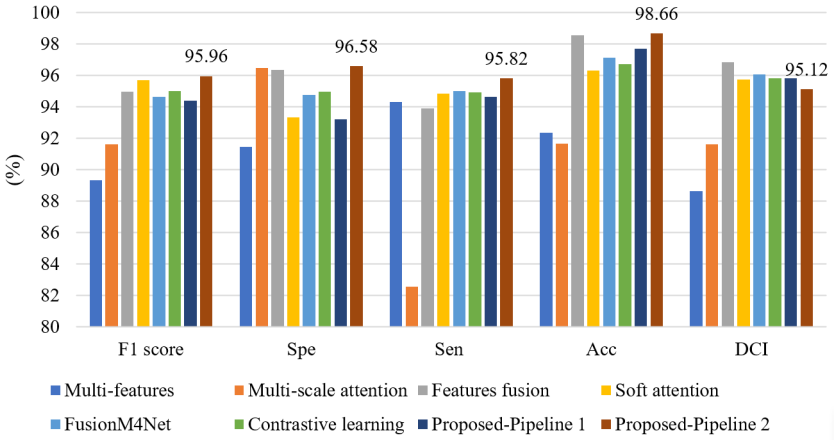

FIGURE 9. Graphical comparison of performance for the proposed skin disease classification system with the recent skin disease classification schemes for the HAM-10000 dataset.

TABLE 3. Performance (%) comparison of proposed skin disease classification system with the recent skin disease classification schemes.

Schemes	HAM 10000					PAD-UFES-20				
	F1 score	Spe	Sen	Acc	DCI	F1 score	Spe	Sen	Acc	DCI
Multi-features [31]	89.32	91.46	94.32	92.34	88.63	87.44	90.42	93.59	90.95	87.15
Multi-scale attention [32]	91.61	96.48	82.57	91.67	91.63	90.32	94.49	81.04	91.48	90.59
Features fusion [33]	94.98	96.37	93.89	98.57	96.84	94.02	95.93	92.63	97.52	96.14
Soft attention [34]	95.69	93.34	94.86	96.32	95.72	94.41	93.13	93.32	95.26	95.42
FusionM4Net [35]	94.62	94.78	95.02	97.14	96.07	93.53	94.56	93.15	95.42	94.90
Contrastive learning [36]	95.01	94.96	94.92	96.73	95.83	93.72	94.83	92.97	95.76	95.31
Proposed-Pipeline 1	94.38	93.21	94.63	97.68	95.82	93.29	92.40	94.25	96.87	95.73
Proposed-Pipeline 2	95.96	96.58	95.82	98.66	95.12	94.52	95.68	95.54	98.10	93.61

algorithms used in lesion classification as illustrated in Table 3. The graphical comparison of F1-score, specificity, sensitivity, accuracy, and DCI between the proposed two pipeline approaches and other recent schemes for the HAM-10000 dataset is illustrated in Fig. 9.

Table 3 also shows the performance comparison of the proposed pipeline-1 and pipeline-2 approaches when evaluated in the PAD-UEFS-20 dataset. For the PAD-UEFS-20 dataset, the proposed pipeline-1 approach results in an F1-score, Specificity, Sensitivity, Accuracy, and DCI of

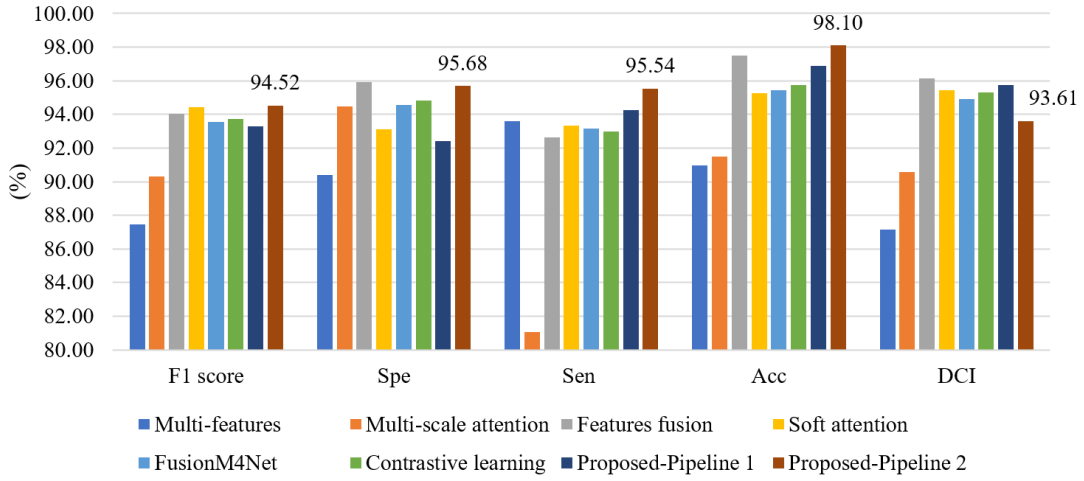

FIGURE 10. Graphical comparison of performance for the proposed skin disease classification system with the recent skin disease classification schemes for the PAD-UFES-20 dataset.

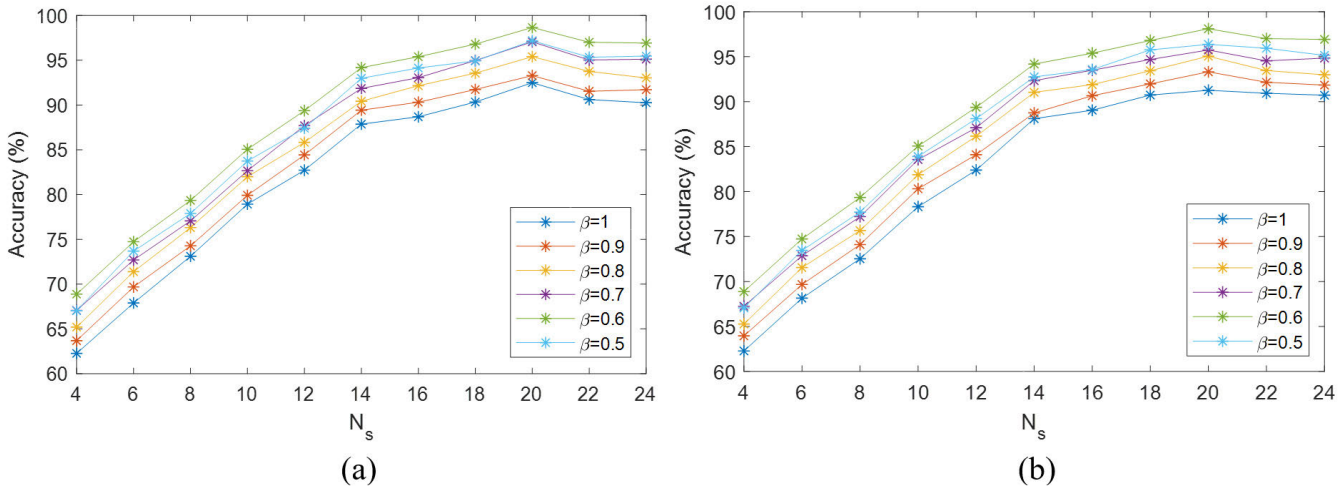

FIGURE 11. Accuracy comparison for different values of N_s and β (a) HAM-10000 dataset (b) PAD-UFES-20 dataset.

TABLE 4. Performance (in %) comparison for the proposed Pipeline-2 structure with different usage of bisectional features.

Feature	HAM-10000					PAD-UFES-20				
	F1 score	Spe	Sen	Acc	DCI	F1 score	Spe	Sen	Acc	DCI
ABCD	94.76	91.53	89.64	92.53	92.64	93.76	90.42	88.13	92.36	91.73
ABCD + Low intense Bisectional	93.74	94.21	93.78	95.12	94.79	92.49	93.94	92.37	94.98	92.55
ABCD + High intense Bisectional	94.15	93.82	94.32	95.39	93.26	92.89	93.74	92.63	95.13	92.78
ABCD + Low and High intense Bisectional	95.96	96.58	95.82	98.66	95.12	94.52	95.68	95.54	98.10	93.61

93.29%, 92.40%, 94.25%, 96.87% and 95.73% respectively. The accuracy of the pipeline-1 approach is 0.67% less than the feature fusion approach. However, the accuracy of the pipeline-2 approach is 0.58% more than the feature fusion approach. In the case of the PAD-UFES-20 dataset, the pipeline-2 approach results in an F1 score, Specificity, Sensitivity, Accuracy, and DCI of 94.52%, 95.68%, 95.54%, 98.10%, and 93.61% respectively. Fig. 10 shows the graphical comparison of performance metrics obtained on the PAD-UEFS-20 dataset.

Fig. 11 shows the variation of accuracy obtained on the pipeline-2 approach for various values of N_s, and β for the datasets HAM-10000 and PAD-UFES-20 dataset. For this analysis, the feature number N_s was varied between 4 to 24 i.e. $N_s = 4, 6, 8, 10, 12, 14, 16, 18,20$, and 24. The parameter β is varied between 0.5 to 1. i.e. $\beta = 0.5, 0.6, 0.7, 0.8, 0.9$, and 1. The pipeline-2 approach results in a maximum accuracy of 98.66% and 98.10% for the HAM-10000 and PAD-UFES-20 with $N_s = 20$, and $\beta = 0.6$. As the N_s value is increased, the accuracy gradually increases

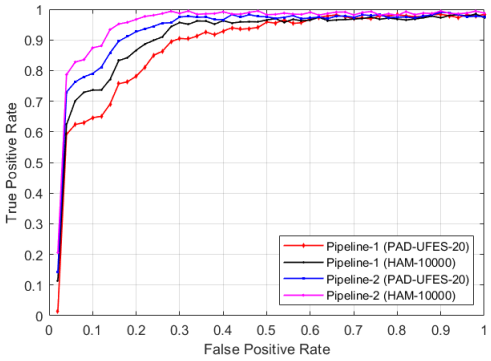

FIGURE 12. ROC analysis in the classification of skin lesion using the pipeline-1 model and pipeline-2 model using two different dataset.

till $N_s = 20$. For further increase in N_s, the accuracy starts to reduce. Also, as the value of β is reduced from 1 to 0.6, the accuracy increases. The maximum accuracy is attained for $\beta = 0.6$. For further reducing the value of β to 0.5, the accuracy reduces.

Fig. 12 illustrates the ROC for the proposed Pipeline-1 and pipeline-2 approach obtained for the HAM-10000 and PAD-UFES-20 dataset. From the graph, it is clear that the proposed pipeline-2 has a higher AUC than the AUC of the proposed pipeline-1 approach. The proposed pipeline-1 approach results in an AUC of 0.961 and 0.953 for the HAM-10000 dataset and PAD-UFES-20 dataset respectively. The proposed pipeline-2 approach results in an AUC of 0.982 and 0.976 for the HAM-10000 dataset and PAD-UFES-20 dataset respectively. The AUC of the pipeline-2 approach is higher than the pipeline-1 approach in both datasets.

Fig. 13 (a), Fig. 13 (b) show the confusion matrices obtained in the classification of skin lesions with the test data using the pipeline-1 and pipeline-2 approach for the HAM-10000 dataset. Fig. 13 (c), Fig. 13 (d) show the confusion matrices obtained in the classification of skin lesions with the test data using the pipeline-1 and pipeline-2 approach for the PAD-UFES-20 dataset. The pipeline-2 approach has a better classification result than the pipeline-1 approach in both the HAM-10000 and PAD-UFES-20 datasets. The Pipeline-1 and Pipeline-2 approach was also evaluated using independent test data. i.e. the model was trained using the HAM-10000 dataset and tested using the PAD-UFES-20 dataset and vice-versa. While training the pipeline-1 and pipeline-2 models using the PAD-UFES-20 dataset training data, the testing was done with the HAM-10000 test data. Pipeline-1 and pipeline-2 results in an accuracy of 94.86% and 95.98% respectively when training using the train data from PAD-UEFS-20 and testing using the test data from the HAM-10000 dataset. While training the pipeline-1 and pipeline-2 models using the HAM-10000 dataset training data, the testing was done with the PAD-UEFS-20 test data. Pipeline-1 and pipeline-2 resulted in an accuracy of 95.12% and 96.04% respectively when training using the train data from HAM-10000 dataset and testing using the test data from the PAD-UEFS-20 dataset. The confusion matrices obtained during the independent test data are provided in Fig. 14.

The pipeline-2 model was evaluated with different combinations of features namely only ABCD features (F_A, F_B, F_C, F_D), ABCD features with low intense Bisectional features (F_A, F_B, F_C, F_D, F_L), ABCD features with High intense Bisectional features (F_A, F_B, F_C, F_D, F_H) and ABCD features with Low and High Bisectional features ($F_A, F_B, F_C, F_D, F_H, F_L$). The evaluation result is provided in Table 4. The usage of only ABCD features results in lower accuracy, while the usage of ABCD features with either low or High intense Bisectional features improves the performance. However, usage of both High and low-intense Bisectional features highly improves the performance in both datasets. With the use of ABCD features, ABCD with low intense Bisectional features, ABCD with High intense Bisectional features, and ABCD with both low and high intense Bisectional features results in an accuracy of 92.53%, 95.12%, 95.39%, and 98.66% respectively in HAM-10000. The accuracy obtained by the pipeline-2 structure using the PAD-UFES-20 dataset is also illustrated in Table 4.

Fig. 15(a) and Fig. 15(b) depicts the time complexity (classification time) comparison of the pipeline-2 approach for different values of N_s, and β in both the HAM-10000 dataset and PAD-UFES-20 dataset respectively. As the value N_s is increased from 2 to 24, for all values of β, the computational complexity increases. The increase in classification time is due to the increase in the number of features used to train and test the SVM classifier. Table 5 illustrates the computation time comparison of the proposed work for $N_s = 18, 20, 22$, and 24. The pipeline-1 approach is independent of the N_s, hence it remains constant. The training time of the AlexNet CNN in training the images using the HAM-10000 and PAD-UFES-20 is estimated as 7632.21s and 3748.5s respectively. The time for testing a single image using the AlexNet CNN is 1.632s and 1.614s for the HAM-10000 and PAD-UFES-20 datasets respectively. Let T_{train} represent the time of training the model. T_{test}, T_{seg}, and T_{fea} represent the time of testing, segmenting, and feature extraction respectively. In the pipeline-2 model, the average time of segmenting the lesion region is 0.34s and 0.321s for the HAM-10000 datasets and PAD-UFES-20 dataset respectively. With $N_s = 20$, the time of training is 921.46s, and the time of extraction of feature, and classification is 0.426s, and 0.346s respectively in HAM-10000 dataset. With $N_s = 20$, the time of training is 468.57s, and the time of extraction of feature, and classification is 0.451s, and 0.339s respectively in the PAD-UFES-20 dataset. As the value of N_s increases the training time, feature extraction time, and classification time increases. This is due to the increase in number of features used in classification.

We intend to further this work in the future utilizing other state-of-the-art CNN models, such as ResNet-152, DeepLab-v3, or Inception-v4, which have demonstrated good results in the classification and segmentation of medical pictures [37]. Additionally, transfer learning and ensembling are other

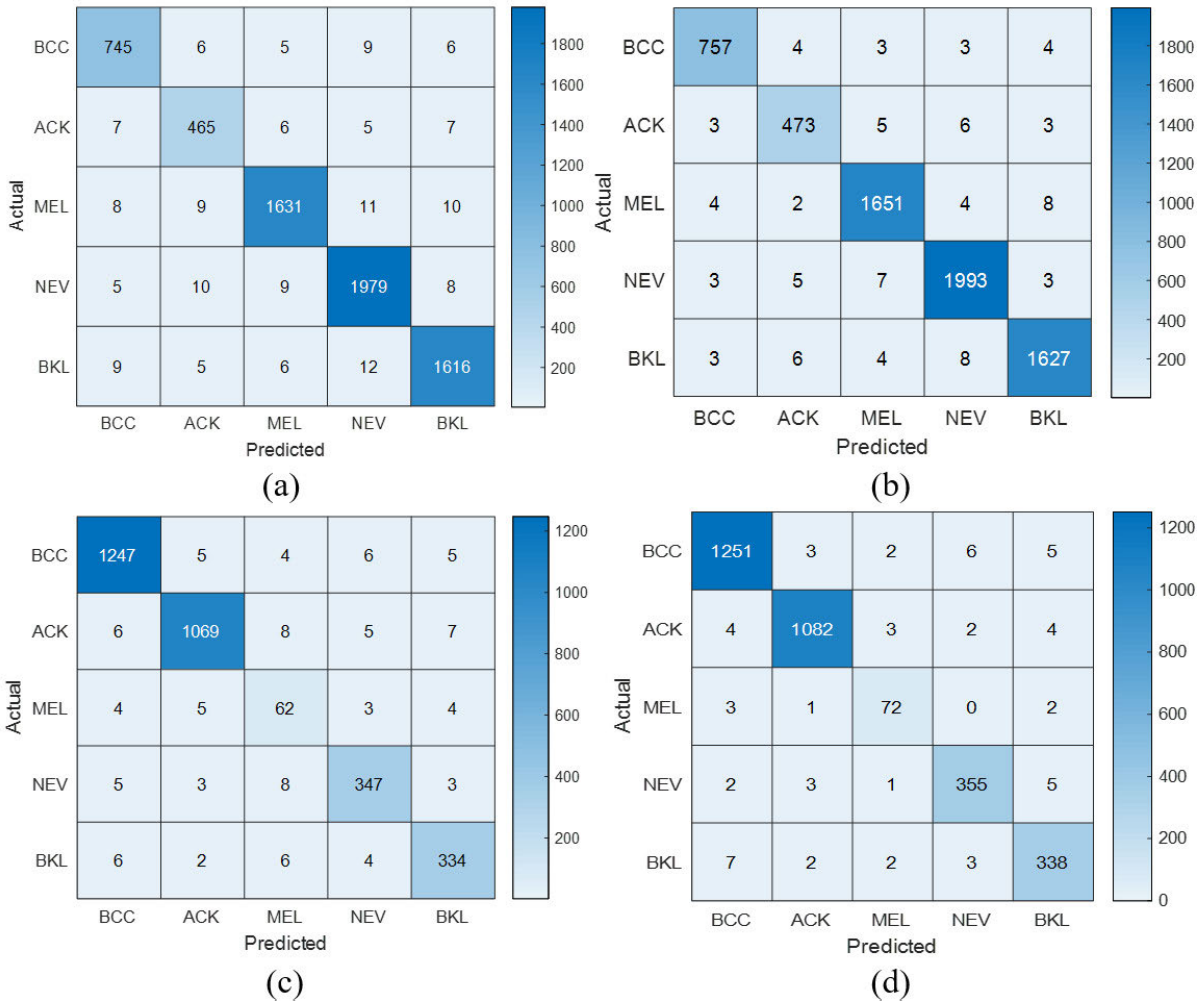

FIGURE 13. Confusion matrices obtained in the classification of skin lesions using the two pipeline structures (a) Pipeline-1 for HAM-10000 (b) Pipeline-2 for HAM-10000 (c) Pipeline-1 for PAD-UFES-20 (d) Pipeline-2 for PAD-UFES-20.

TABLE 5. Time complexity (in seconds) comparison of proposed Pipeline-1 and Pipeline-2 model for different values of N_s.

Dataset	N_s	Pipeline-1		Pipeline-2			
		T_{train}	T_{test}	T_{train}	T_{seg}	T_{fea}	T_{test}
HAM 10000	18	7632.21	1.632	896.64	0.34	0.394	0.321
	20			921.46		0.426	0.346
	22			983.45		0.432	0.368
	24			1021.53		0.513	0.392
PAD-UFES-20	18	3748.5	1.614	453.12	0.321	0.42	0.317
	20			468.57		0.451	0.339
	22			499.15		0.47	0.358
	24			573.94		0.552	0.381

strategies for enhancing generalization performance. Transfer learning is the process of administering the knowledge gained from one problem-solving experience to address another [6]. In the field of CNNs, transfer learning frequently involves either fine-tuning potent pre-trained deep learning models for the intended job or employing a CNN as a fixed feature extractor. The main benefits of transfer learning include the ability to overcome some significant CNN-related challenges, such as the need for powerful hardware to support their computational complexity, an appropriate weights initialization, and careful network architecture design, in addition to typically allowing for better results. In ensemble learning, many CNN models are used to achieve superior predictive performance compared to any one of the individual models. Diagnosis of skin lesions at its early stage is essential for effective treatment and better patient outcomes, especially for Melanoma. To sum up, the goal of this work is to serve as a solid foundation for the creation

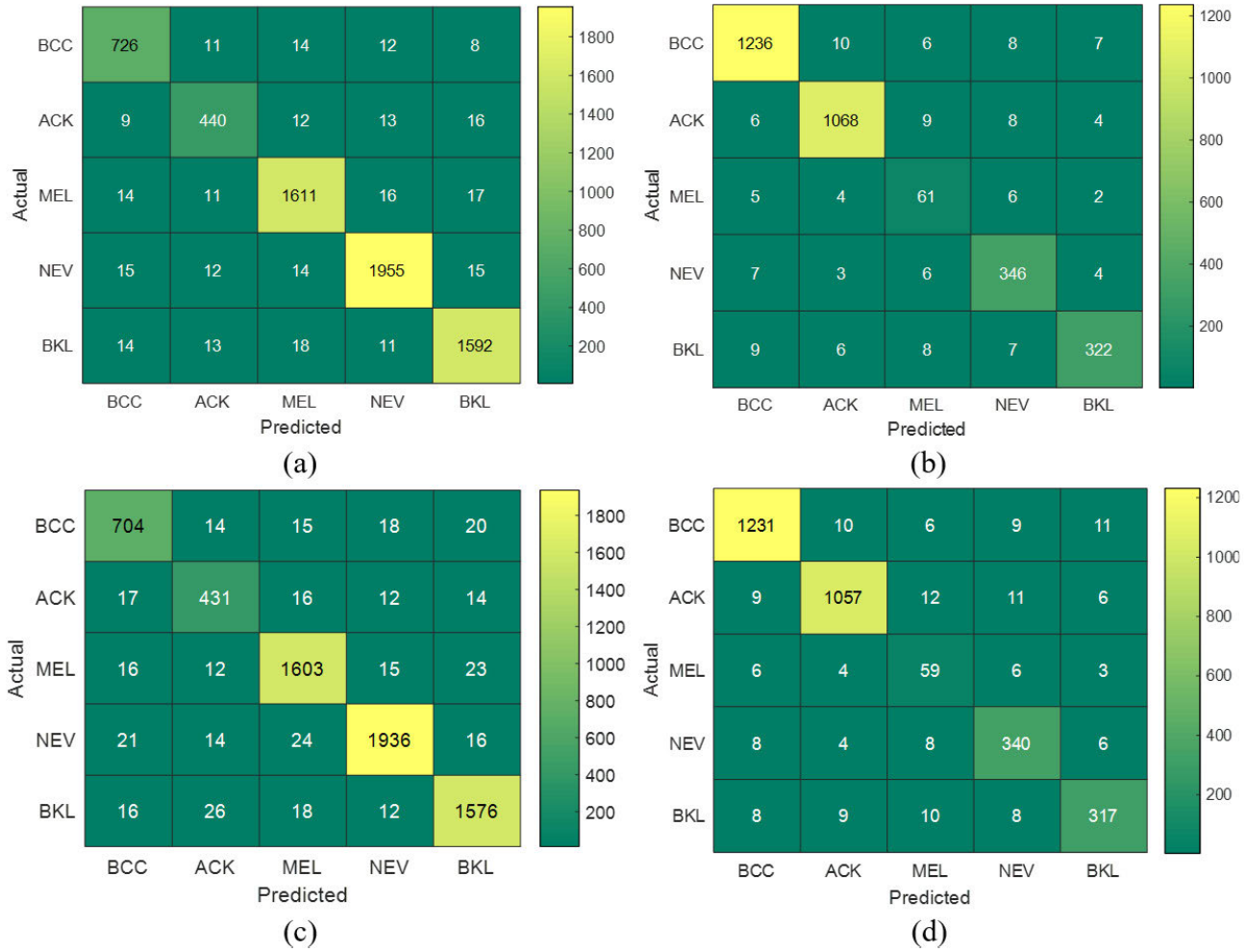

FIGURE 14. Confusion matrices obtained in the classification of skin lesions using the two pipeline structures (a) Pipeline-2 (Trained in PAD-UFES-20 train data and tested in HAM-10000 test data) (b) Pipeline-2 (Trained in HAM-10000 train data and tested in PAD-UFES-20 test data) (c) Pipeline-1 (Trained in PAD-UFES-20 train data and tested in HAM-10000 test data) (d) Pipeline-1 (Trained in HAM-10000 train data and tested in PAD-UFES-20 test data).

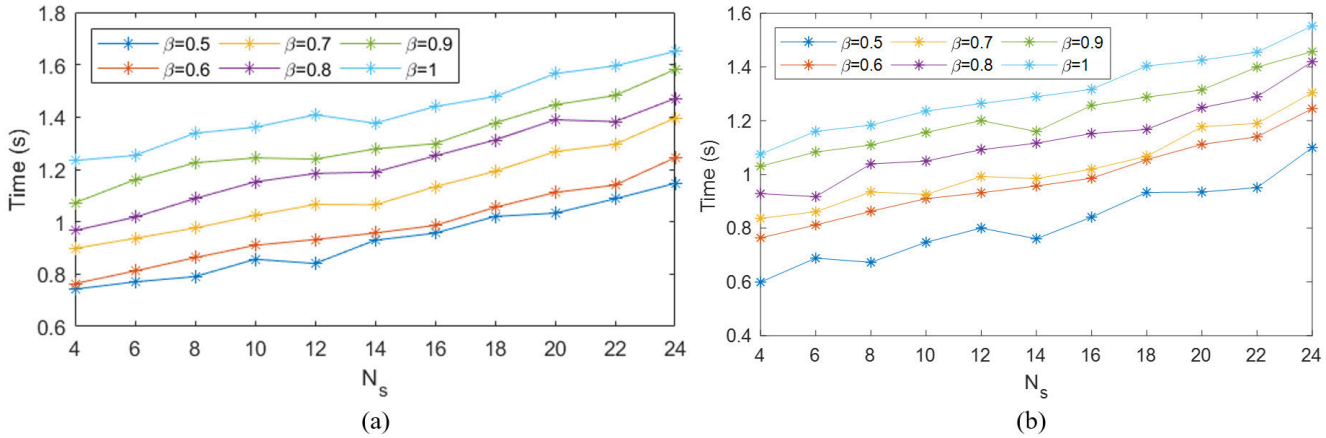

FIGURE 15. Time complexity comparison for different values of N_s and β (a) HAM-10000 dataset (b) PAD-UFES-20 dataset.

of sophisticated systems for classifying skin lesions that are capable of democratizing and spreading access to medical care to dramatically lower medical expenditures and save many lives through early identification.

V. CONCLUSION

In this work, the pipelines for classification were constructed and an automatic classification system of dermatoscopic images from the HAM10000 dataset and PAD-UFES-20

was reported. The system in this work is built with two distinct pipelines: one utilizes the AlexNet CNN for image classification, and the other one employs the SVM machine learning model to classify images after segmenting them and collecting some features from the lesion region using the ABCDT analysis. The pipeline-1 and pipeline-2 results in an accuracy of 97.68% and 98.66% respectively for the HAM-10000 dataset. In the case of the PAD-UFES-20 dataset, the pipeline-1 and pipeline-2 structure results in an accuracy of 96.87% and 98.10% respectively. Based on these findings, it can be concluded that performance levels that resemble those attained using deep learning approaches can be attained by combining an improved classifier with cutting-edge segmentation techniques and feature extraction strategy.

REFERENCES

[1] M. A. Kassem, K. M. Hosny, and M. M. Fouad, "Skin lesions classification into eight classes for ISIC 2019 using deep convolutional neural network and transfer learning," *IEEE Access*, vol. 8, pp. 114822–114832, 2020.

[2] H. Alquran, I. A. Qasmieh, A. M. Alqudah, S. Alhammouri, E. Alawneh, A. Abughazaleh, and F. Hasayen, "The melanoma skin cancer detection and classification using support vector machine," in *Proc. IEEE Jordan Conf. Appl. Electr. Eng. Comput. Technol. (AEECT)*, Oct. 2017, pp. 1–5.

[3] N. K. A. Abbadi, "Psoriasis detection using skin color and texture features," *J. Comput. Sci.*, vol. 6, no. 6, pp. 648–652, Jun. 2010.

[4] M. A. Khan, K. Muhammad, M. Sharif, T. Akram, and V. H. C. D. Albuquerque, "Multi-class skin lesion detection and classification via teledermatology," *IEEE J. Biomed. Health Informat.*, vol. 25, no. 12, pp. 4267–4275, Dec. 2021.

[5] S. H. Krishnan, C. Vishwa, M. Suchetha, A. Raman, R. Raman, S. Sehastrajit, and D. E. Dhas, "Comparative performance of deep learning architectures in classification of diabetic retinopathy," *Int. J. Ad Hoc Ubiquitous Comput.*, vol. 1, no. 1, p. 1, 2023.

[6] Q. Sun, C. Huang, M. Chen, H. Xu, and Y. Yang, "Skin lesion classification using additional patient information," *BioMed Res. Int.*, vol. 2021, pp. 1–6, Apr. 2021.

[7] M. Suchetha, N. S. Ganesh, R. Raman, and D. E. Dhas, "Region of interest-based predictive algorithm for subretinal hemorrhage detection using faster R-CNN," *Soft Comput.*, vol. 25, no. 24, pp. 15255–15268, Dec. 2021.

[8] S. Das, K. Kharbanda, M. Suchetha, R. Raman, and E. Dhas, "Deep learning architecture based on segmented fundus image features for classification of diabetic retinopathy," *Biomed. Signal Process. Control*, vol. 68, Jul. 2021, Art. no. 102600.

[9] P. Kharazmi, M. I. AlJasser, H. Lui, Z. J. Wang, and T. K. Lee, "Automated detection and segmentation of vascular structures of skin lesions seen in dermoscopy, with an application to basal cell carcinoma classification," *IEEE J. Biomed. Health Informat.*, vol. 21, no. 6, pp. 1675–1684, Nov. 2017.

[10] M. Shamsul Arifin, M. Golam Kibria, A. Firoze, M. Ashraful Amini, and H. Yan, "Dermatological disease diagnosis using color-skin images," in *Proc. Int. Conf. Mach. Learn. Cybern.*, vol. 5, Jul. 2012, pp. 1675–1680.

[11] V. Anand, S. Gupta, D. Koundal, S. R. Nayak, J. Nayak, and S. Vimal, "Multi-class skin disease classification using transfer learning model," *Int. J. Artif. Intell. Tools*, vol. 31, no. 2, Mar. 2022, Art. no. 2250029.

[12] R. Muthalagu, M. M. Musheer, K. Nandhini, and N. Saranraj, "Type of skin disease identification by machine learning using Python," *Int. J. Sci. Eng. Develop. Res.*, vol. 6, no. 3, pp. 498–503, Mar. 2021.

[13] V. R. Allugunti, "A machine learning model for skin disease classification using convolution neural network," *Int. J. Comput., Program. Database Manage.*, vol. 3, no. 1, pp. 141–147, Jan. 2022.

[14] M. Q. Khan, A. Hussain, S. U. Rehman, U. Khan, M. Maqsood, K. Mehmood, and M. A. Khan, "Classification of melanoma and nevus in digital images for diagnosis of skin cancer," *IEEE Access*, vol. 7, pp. 90132–90144, 2019.

[15] X. Zhang, S. Wang, J. Liu, and C. Tao, "Towards improving diagnosis of skin diseases by combining deep neural network and human knowledge," *BMC Med. Informat. Decis. Making*, vol. 18, no. S2, pp. 69–76, Jul. 2018.

[16] C.-Y. Zhu, Y.-K. Wang, H.-P. Chen, K.-L. Gao, C. Shu, J.-C. Wang, L.-F. Yan, Y.-G. Yang, F.-Y. Xie, and J. Liu, "A deep learning based framework for diagnosing multiple skin diseases in a clinical environment," *Frontiers Med.*, vol. 8, Apr. 2021, Art. no. 626369.

[17] S. Inthiyaz, B. R. Altahan, S. H. Ahammad, V. Rajesh, R. R. Kalangi, L. K. Smirani, M. A. Hossain, and A. N. Z. Rashed, "Skin disease detection using deep learning," *Adv. Eng. Softw.*, vol. 175, 2023, Art. no. 103361.

[18] M. Cullell-Dalmau, S. Noé, M. Otero-Viñas, I. Meić, and C. Manzo, "Convolutional neural network for skin lesion classification: Understanding the fundamentals through hands-on learning," *Frontiers Med.*, vol. 8, Mar. 2021, Art. no. 644327.

[19] A. Krizhevsky, I. Sutskever, and G. E. Hinton, "ImageNet classification with deep convolutional neural networks," *Commun. ACM*, vol. 60, no. 6, pp. 84–90, May 2017.

[20] R. D. Seeja and A. Suresh, "Deep learning based skin lesion segmentation and classification of melanoma using support vector machine (SVM)," *Asian Pacific J. Cancer Prevention*, vol. 20, no. 5, pp. 1555–1561, May 2019.

[21] S. S. Samsudin, H. Arof, S. W. Harun, A. W. A. Wahab, and M. Y. I. Idris, "Skin lesion classification using multi-resolution empirical mode decomposition and local binary pattern," *PLoS ONE*, vol. 17, no. 9, Sep. 2022, Art. no. e0274896.

[22] P. N. Srinivasu, J. G. Sivasai, M. F. Ijaz, A. K. Bhoi, W. Kim, and J. J. Kang, "Classification of skin disease using deep learning neural networks with MobileNet V2 and LSTM," *Sensors*, vol. 21, no. 8, p. 2852, Apr. 2021.

[23] P. Musa, F. A. Rafi, and M. Lamsani, "A review: Contrast-limited adaptive histogram equalization (CLAHE) methods to help the application of face recognition," in *Proc. 3rd Int. Conf. Informat. Comput. (ICIC)*, Oct. 2018, pp. 1–6.

[24] M. A. Kassem, K. M. Hosny, R. Damaševič ius, and M. M. Eltoukhy, "Machine learning and deep learning methods for skin lesion classification and diagnosis: A systematic review," *Diagnostics*, vol. 11, no. 8, p. 1390, Jul. 2021.

[25] S. Joseph and O. O. Olugbara, "Preprocessing effects on performance of skin lesion saliency segmentation," *Diagnostics*, vol. 12, no. 2, p. 344, Jan. 2022.

[26] D. Z. Karim and T. A. Bushra, "Detecting lung cancer from histopathological images using convolution neural network," in *Proc. IEEE Region 10 Conf. (TENCON)*, Dec. 2021, pp. 626–631.

[27] A. Agarwal, A. Issac, M. K. Dutta, K. Riha, and V. Uher, "Automated skin lesion segmentation using K-means clustering from digital dermoscopic images," in *Proc. 40th Int. Conf. Telecommun. Signal Process. (TSP)*, Jul. 2017, pp. 743–748.

[28] F. Adjed, S. J. Safdar Gardezi, F. Ababsa, I. Faye, and S. Chandra Dass, "Fusion of structural and textural features for melanoma recognition," *IET Comput. Vis.*, vol. 12, no. 2, pp. 185–195, Mar. 2018.

[29] N. Codella, V. Rotemberg, P. Tschandl, M. Emre Celebi, S. Dusza, D. Gutman, B. Helba, A. Kalloo, K. Liopyris, M. Marchetti, H. Kittler, and A. Halpern, "Skin lesion analysis toward melanoma detection 2018: A challenge hosted by the international skin imaging collaboration (ISIC)," 2019, *arXiv:1902.03368*.

[30] A. G. C. Pacheco and R. A. Krohling, "The impact of patient clinical information on automated skin cancer detection," *Comput. Biol. Med.*, vol. 116, 2020, Art. no. 103545.

[31] S. Benyahia, B. Meftah, and O. Lézoray, "Multi-features extraction based on deep learning for skin lesion classification," *Tissue Cell*, vol. 74, Feb. 2022, Art. no. 101701.

[32] S. Qian, K. Ren, W. Zhang, and H. Ning, "Skin lesion classification using CNNs with grouping of multi-scale attention and class-specific loss weighting," *Comput. Methods Programs Biomed.*, vol. 226, Nov. 2022, Art. no. 107166.

[33] S. Maqsood and R. Damaševič ius, "Multiclass skin lesion localization and classification using deep learning based features fusion and selection framework for smart healthcare," *Neural Netw.*, vol. 160, pp. 238–258, Mar. 2023.

[34] A. N. Omeroglu, H. M. A. Mohammed, E. A. Oral, and S. Aydin, "A novel soft attention-based multi-modal deep learning framework for multi-label skin lesion classification," *Eng. Appl. Artif. Intell.*, vol. 120, Apr. 2023, Art. no. 105897.

[35] P. Tang, X. Yan, Y. Nan, S. Xiang, S. Krammer, and T. Lasser, "FusionM4Net: A multi-stage multi-modal learning algorithm for multi-label skin lesion classification," *Med. Image Anal.*, vol. 76, Feb. 2022, Art. no. 102307.

[36] S. Liang, S. Tian, X. Kang, D. Zhang, W. Wu, and L. Yu, "Skin lesion classification base on multi-hierarchy contrastive learning with Pareto optimality," *Biomed. Signal Process. Control*, vol. 86, Sep. 2023, Art. no. 105187.
[37] Y. Zhao, B. Hu, Y. Wang, X. Yin, Y. Jiang, and X. Zhu, "Identification of gastric cancer with convolutional neural networks: A systematic review," *Multimedia Tools Appl.*, vol. 81, no. 8, pp. 11717–11736, Mar. 2022.

V. S. S. BALA TRIPURA SATHVIKA received the B.Tech. degree in electronics and communication engineering from Vellore Institute of Technology, Chennai. Her research interests include deep learning, big data, and data analytics.

NAGILLA ANMISHA received the B.Tech. degree in electronics and communication engineering from Vellore Institute of Technology, Chennai. Her research interests include data analytics and deep learning.

VADA THANMAYI received the B.Tech. degree in electronics and communication engineering from Vellore Institute of Technology, Chennai. Her research interests include data analytics and deep learning.

M. SUCHETHA (Senior Member, IEEE) received the Ph.D. degree in biomedical. Her Ph.D. thesis was titled "Empirical Mode Decomposition-Based Denoising and Classification Techniques Applied to Electrocardiogram Signals." She is currently the Deputy Director of the Centre for Healthcare Advancements, Innovation and Research, VIT University. She is the Principal Investigator for a funded project by ISRO and other funded projects. She has published more than 70 articles in journals, authored four books, and filed several patents. Her research interests include wearable devices, signal/image processing techniques in biomedical, AI, big data analytics for healthcare, and developing non-invasive devices. She is a Life Member of ISTE, a Senior Member of the IEEE Engineering in Medicine and Biology Society (EMBS), and a Faculty Advisor of the IEEE Robotics and Automation Society.

D. EDWIN DHAS received the bachelor's degree in electronics and communication engineering from the Ponjesly College of Engineering, affiliated to Anna University, Chennai, India, and the master's degree from the C.S.I Institute of Technology, affiliated to Anna University, India. He is currently pursuing the Ph.D. degree with VIT University, Chennai, India. His research interests include bio-signal processing, radar signal processing, image processing, and adaptive filtering techniques.

S. SEHASTRAJIT is currently pursuing the B.Tech. degree with Vellore Institute of Technology. His research interests include artificial intelligence applications and developing ML/DL algorithms. He was a recipient of the "Student of the Year" Award consecutively for two years from USA UnivQuest, Global SOTY Foundation.

SATHYANARAYANAN N. AAKUR (Member, IEEE) received the B.Eng. degree in electronics and communication engineering from Anna University, Chennai, India, in 2013, and the M.S. degree in management information systems and the Ph.D. degree in computer science from the University of South Florida, Tampa, in 2015 and 2019, respectively. He is currently an Assistant Professor with the Department of Computer Science, Auburn University. His research interests include self-supervised learning, commonsense reasoning for visual understanding, and deep learning applications for genomics. He was a recipient of the National Science Foundation CAREER Award, in 2022. He served as an Associate Editor for IEEE Robotics and Automation Letters, since 2021.